Estimating the effect of cooperative versus uncooperative strategies of COVID-19 vaccine allocation: a modeling study

Matteo Chinazzi [1], Jessica T. Davis[1], Natalie E. Dean[2], Kunpeng Mu[1],
Ana Pastore y Piontti[1], Xinyue Xiong[1], M. Elizabeth Halloran[3,4],
Ira M. Longini Jr.[2], Alessandro Vespignani[1,5,†]

[1]Laboratory for the Modeling of Biological and Socio-technical Systems,
Northeastern University, Boston, MA USA
[2]Department of Biostatistics, College of Public Health and Health Professions,
University of Florida, Gainesville, USA
[3]Fred Hutchinson Cancer Research Center, Seattle, WA, USA
[4]Department of Biostatistics, University of Washington, Seattle, WA. USA
[5]ISI Foundation, Turin, Italy
[†]To whom correspondence should be addressed; E-mail: a.vespignani@northeastern.edu.

We use a global metapopulation transmission model to study the effect of different COVID-19 vaccine allocation strategies across countries of the world. In the two scenarios considered, 3 billion doses are distributed worldwide. In the *uncooperative allocation scenario*, the first 2 billion doses are co-opted by a list of high-income countries, while the third billion is distributed equally around the world. In the *cooperative allocation scenario*, all the 3 billion doses are distributed to all countries proportionally to their population. To avoid uncontrolled assumptions and unknowns about the future course of the COVID-19 pandemic, we consider a counterfactual scenario analyzing what would have happened if the vaccine had been available on March 16th, 2020. The model considers a single dose vaccine that is effective two weeks after administration. We find that the cooperative and uncooperative strategy would have averted 61% and 33% of the deaths globally through September 1st, 2020, respectively, when the vaccine is 80% effective, and 57% and 30% deaths when the vaccine is 65% effective.

Introduction

As of September 12th, 2020 the COVID-19 pandemic has recorded worldwide 28,525,510 confirmed infections and has killed more than 916,000 people (*1*). As the number of confirmed COVID-19 cases increased a large number of affected countries have been forced to adopt non-pharmaceutical interventions at an unprecedented scale that generate economic loss and widespread disruption to social life. As the pandemic is still spreading the entire world looks anxiously to the development of vaccines as the solution to the COVID-19 unprecedented crisis. Any effective COVID-19 vaccine, however will be initially scarce, raising the issue of how doses will be distributed between different countries. While on one side many organizations are advocating for a fair and equitable distribution of the available vaccine, some countries are already reserving large amount of doses, even before the vaccine has been cleared for use. In order to investigate the effect of different approaches to the distribution of COVID-19 vaccines, we use a large-scale computational model to compare two international allocation strategies: one in which initially only a limited number of countries benefit from a large vaccine stockpile, and a second one in which vaccines supplies are equitably shared worldwide proportional to population.

To study the spatial and temporal spread of COVID-19, we use the Global Epidemic and Mobility Model (GLEAM), an individual-based, stochastic, and spatial epidemic model (*2–6*). The model was previously used to characterize the early stage of the COVID-19 epidemic in mainland China and the effect of travel restrictions on infections exported to other global regions (*7*). GLEAM generates an ensemble of possible epidemics described by the number of newly generated infections, the time of disease arrival in different regions of the world, and the number of infected travelers. The model divides the global population into more than $3,200$ subpopulations in roughly 200 different countries and territories. The airline transportation data encompass daily origin-destination traffic flows from the Official Aviation Guide (OAG) and the International Air Transport Association (IATA) databases (*8, 9*), whereas ground mobility flows are derived from the analysis and modeling of data collected from the statistics offices of 30 countries on five continents (*2, 3*).

The transmission dynamics take place within each subpopulation and assume an SLIR-like compartmentalization scheme for the disease progression similar to those used in several large scale models of SARS-CoV-2 transmission (*10–15*). Each individual, at any given point in time, is assigned to a compartment corresponding to their particular disease-related state (e.g., susceptible, latent, infectious, removed) (*7*). This state also controls the individual's ability to travel (details in Materials and Methods). Individuals transition between compartments through stochastic chain binomial processes. Susceptible individuals can acquire the virus through contacts with individuals in the infectious category and can subsequently become latent (i.e., infected but not yet able to transmit the infection). Vaccinated individuals transition in a separate removed compartment if immunity is acquired. This last stochastic process models an all-or-none protection to achieve the desired 80% vaccine efficacy. The process of infection is modeled using age-stratified contact patterns at the state level (*16*). Latent individuals progress to the in-

fectious stage at a rate inversely proportional to the latent period, and infectious individuals progress to the removed stage at a rate inversely proportional to the infectious period. The sum of the mean latent and infectious periods defines the generation time. Removed individuals are those who can no longer infect others. To estimate the number of deaths, we use the age-stratified infection fatality ratios from (*17*). We are not considering co-morbidities and other potential risk factors that might affect mortality across different countries. At this stage, the transmission model does not account for heterogeneities due to age differences in susceptibility to the SARS-CoV-2 infection. This is an intense area of discussion at the moment (*18–20*).

We assume a start date of the epidemic in Wuhan, China, that falls between November 15, 2019 and December 1, 2019, with 20 initial infections (*7, 15, 21–24*). The model generates an ensemble of possible epidemic realizations and is calibrated using Approximate Bayesian Computation (ABC) methods (*25*) based on the observed international importations from mainland China through January 21, 2020 (*7*) and using a generation time $T_g = 6.5$ days. Only a fraction of imported cases are detected at the destination (*26*). According to the estimates proposed in (*27*), we stratify the detection capacity of countries into three groups: high, medium and low surveillance capacity according to the Global Health Security Index (*28*), and assume asymptomatic infections in January were not detected (see Materials and Methods). The model calibration does not consider correlated importations (family travel) and assumes that travel probabilities are homogeneous across all individuals in each subpopulation. The model accounts for international travel restrictions according to available data on traffic reduction and government issued policies. We report the details of the model in the Materials & Methods section.

The vaccine administration is modeled as follows. First, the daily stockpile of the vaccine is shipped to each location according to the vaccine allocation strategy. Once vaccine doses are available in a location, a random binomial draw is performed to distribute the available doses to the different age groups according to a probability that is proportional to the age-specific infection fatality rate of each age group (*47*). Vaccine inoculation is modeled at the single individual level according to the available doses in each age bracket. An additional random draw for each vaccine inoculation will establish if the vaccine will be effective. This last stochastic process models an all-or-none protection to achieve the desired vaccine efficacy. For example, for a vaccine that is 80% effective, 80% of the vaccinated individuals are completely protected after two weeks from receiving the vaccine, while 20% receive no protection. Vaccine doses are administered to individuals irrespective of their clinical history, with the exception of currently infectious symptomatic individuals.

Vaccine allocation scenarios

In this analysis we consider three scenarios: a) a *baseline* reference scenario in which no vaccine is administered; b) an *uncooperative vaccine allocation*; and c) a *cooperative vaccine allocation*. One of the main problems in modeling the effects of vaccine allocation is to define

scenarios for the evolution of the COVID-19 pandemic once the vaccine doses will be available, most likely in the early months of 2021. We therefore considered a different approach in which we assume that the vaccine would have been available by mid March 2020. In this way we can consider the evolution of the epidemic to follow the trajectory initially observed in 2020, and model the interventions adopted by each country according to actual data concerning travel restrictions, non-pharmaceuticals interventions and public health policies such as school closure (as detailed in the Material and Methods section).

In both vaccine allocation strategies we assume that a stockpile of 3 billion doses in total is distributed over the course of 6 months starting March 16th, 2020. Additionally, we assume that one week is needed to start the distribution at a global scale. Currently, no interim analysis of phase 3 trials of several candidates vaccines are available. We have therefore assumed a single dose of an all-or-none vaccine that is effective two weeks after administration. A sensitivity analysis for vaccine efficacy is performed and two different scenarios are considered in this study. One in which vaccine efficacy is 80% and one in which it is 65%. The weekly number of available doses, globally, is assumed to be 125,000,000. The model also considers that problems in logistics may delay the planned availability of vaccine doses, assuming that up to 15% of the doses might not be administered by September 1st, 2020 as planned.

We consider the two following vaccine allocation strategies:

- *Uncooperative allocation scenario*: the first 2 billion doses of the vaccine are administered only to the list of countries reported in Table 2 and doses are pro-rated with respect to the population size of each country.

- *Cooperative allocation scenario* assumes that the first 2 billion doses are distributed proportionally to the population of the countries.

In both scenarios the remaining 1 billion doses are distributed to all countries (including the list of priority countries) proportionally to their population.

The two above scenarios are not an exhaustive analysis of possible fair frameworks for international vaccine allocations. As the discussion about an ethical and equitable international distribution of vaccines progresses, novel distribution frameworks based on geographically targeted approaches aimed at reducing direct and indirect health impacts and deaths are developed. The presented results are therefore not to be considered as the analysis of an optimal strategy but just as a first step of an extensive analysis of ethical frameworks for global vaccine allocation (*46*).

Results and Discussion

To estimate the effect of the cooperative and uncooperative COVID-19 vaccine allocation strategies we have computed the median number of deaths in each different scenario and calculated the proportion of averted deaths with respect to the baseline scenario with no vaccine distribution. More specifically, the proportion of globally averted deaths (reported in Figure 1) is
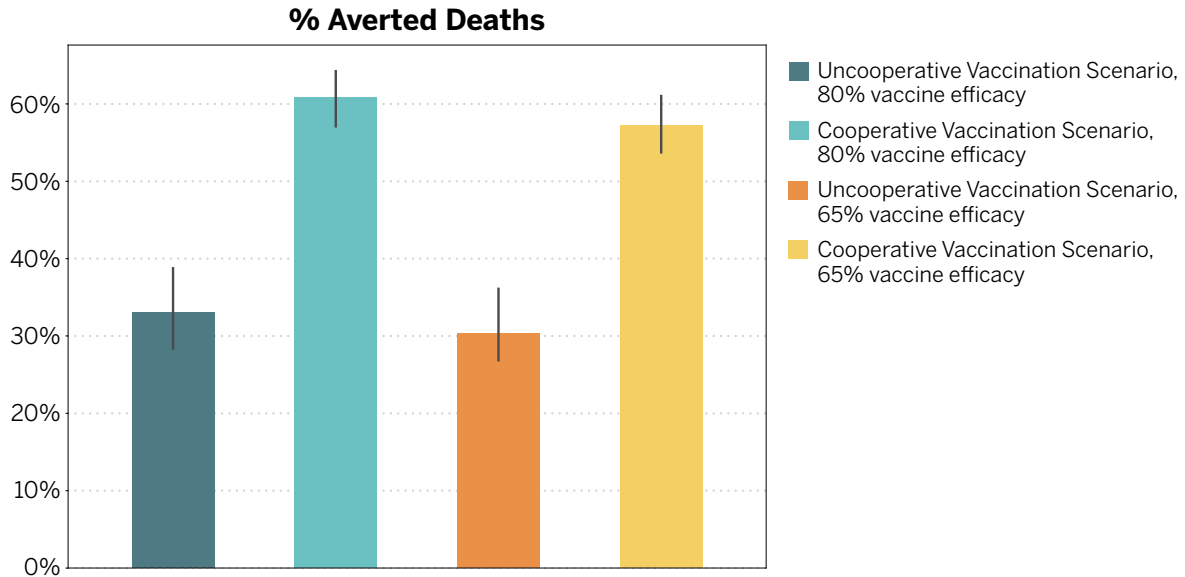
Figure 1: **Share of globally averted deaths as of September 1st, 2020.** In this figure we report the share of averted deaths computed as one minus the ratio of the median number of worldwide deaths that occurred in the uncooperative (or cooperative) allocation scenario and the median number of deaths that occurred in the baseline (no vaccine) scenario.

computed as one minus the ratio of the median number of worldwide deaths that occurred in the uncooperative (or cooperative) allocation scenario and the median number of deaths that occurred in the baseline (no vaccine) scenario. The median values refer to the outcome of the 6,000 identically initialized numerical realizations of the model analyzed for each scenario. We find that for a 80% vaccine efficacy the uncooperative vaccine allocation strategy would avert 33% [95CI 28%–39%] deaths, while the cooperative allocation strategy is estimated to avert 61% [95CI 57%–64%] deaths. If a 65% vaccine efficacy is assumed, the percentages of averted deaths in the two scenarios become 30% [95CI 27%–36%] in the uncooperative scenario and 57% [95CI 54%–61%] in the cooperative scenario.

It is important to stress that while at the global level the estimated number of averted deaths with the cooperative strategy is twice the one in the uncooperative strategy, the uncooperative strategy is providing a modest gain in averted deaths for the countries who can access the vaccine stockpile when compared to the possible loss suffered by non-priority countries. For instance, for an 80% vaccine efficacy, in Western Europe, the uncooperative strategy indicates a proportion of averted deaths of 74%, while the cooperative strategy achieves a 55% averted deaths; in Northern America the uncooperative strategy averted 67% deaths compared to the 53% of the cooperative strategy. This however has to be contrasted with other regions such as Western Africa where the uncooperative and cooperative strategies achieve 13% and 93% averted deaths, respectively, while in South-Eastern Asia they achieve 5% and 62% averted

deaths, respectively. It is worth remarking that the model's numerical simulations explore the many possible paths of the epidemic given the same set of non-pharmaceutical interventions and other policies implemented across the world. Thus, the analysis provided here must be considered as a statistical description of the many possible statistical trajectories of the epidemic once the vaccine distribution is started. The analysis thus provides general information concerning the statistical effectiveness of the different vaccinale allocation startegies. For this reason we report the proportion of averted deaths instead of the number of averted deaths, a number that could vary considerably across the different epidemic histories explored numerically.

Our analysis as with all modeling exercises has limitations and requires certain assumptions. The model parameters are based on the current knowledge of SARS-CoV-2 and although the model is stable to variations in these parameters, more information on the key characteristics of the disease might impact the results of this study. At this stage, the number of available vaccine doses, the mechanism of vaccine efficacy, and the distribution capacity are best guesses based on expert assessment and priors mostly based on flu vaccine distribution. It is also likely that with ongoing vaccination programs some countries would have opted for different policies than those implemented from April to August, 2020. Our modeling approach instead considers the policies in place during the course of the COVID-19 epidemic independently of the effect of the vaccination distribution programs.

Acknowledgements

Data and materials availability

Proprietary airline data are commercially available from Official Aviation Guide (OAG) and IATA databases. The GLEAM model is publicly available at http://www.gleamviz.org/.

Materials and Methods

Here, we provide the details about the model calibration, present the sensitivity analysis of some key parameters, and describe the details of the importation sources estimation. We also include an analysis of the empirical data, several indicators (air traffic, population, density), and the data obtained from the model.

Global Epidemic and Mobility Model
We adopt the Global Epidemic and Mobility model (GLEAM), a stochastic spatial epidemic model based on a metapopulation approach that has been used and published previously (*2, 3*). In the model, the world

is divided into over 3,200 geographic subpopulations constructed using a Voronoi tessellation of the Earth's surface. Subpopulations are centered around major transportation hubs (e.g. airports) and consist of cells with a resolution of 15 x 15 arc minutes (approximately 25 x 25 kilometers). High resolution data are used to define the population of each cell (*29*). Other attributes of individual subpopulations, such as age-specific contact patterns, health infrastructure, etc., are added according to available data (*16*).

GLEAM integrates a human mobility layer - represented as a network - that uses both short-range (i.e. commuting) and long-range (i.e. flights) mobility data from the Offices of Statistics for 30 countries on 5 continents as well as the Official Aviation Guide (OAG) and IATA databases (updated in 2019) (*8,9*). The air travel network consists of the daily passenger flows between airport pairs (origin and destination) worldwide mapped to the corresponding subpopulations. We define a worldwide homogeneous standard for GLEAM to overcome differences in the spatial resolution of the commuting data across different countries. Where information is not available, the short-range mobility layer is generated synthetically by relying on the "gravity law" or the more recent "radiation law" both calibrated using real data (*30*). These approaches assume more frequent traveling to nearby or closer subpopulations and less frequent traveling to distant locations. In Fig. 2 we show a representation of the geographical resolution of the model and the mobility network for the world.

Initial conditions are set specifying the number and location of individuals capable of transmitting the infection. GLEAM is then able to track over time the proportion of the population in each disease compartment for all subpopulations. At the start of each simulated day, travelers move to their destinations via the flight network. The probability of air travel changes from day to day, varies by age group, and accounts for the effects of location specific airline traffic reductions and restrictions. Short-range mobility (i.e. commuting) varies between workdays and weekends, by age group, and by disease status. Each full day is simulated using 12 distinct time steps, and this process is repeated for every simulated day. Individuals and their traveling patterns are tracked as shown in the flow diagram for the GLEAM algorithm (Fig. 3).

The combined population structure and mobility network create a synthetic world that is used to simulate the unfolding dynamics of the epidemic. The infection dynamics occur within each subpopulation. We adopt a classic $SLIR$ model in which individuals can be classified into four compartments: susceptible, latent, infectious, or removed. Susceptible individuals become latent through interactions with infectious individuals. During both the latent and infectious stages we assume that individuals are able to travel. Following the infectious period, individuals then progress into the removed compartment where they are no longer able to infect others, meaning they have either recovered, been hospitalized, isolated or have died. Individuals transition between compartments using stochastic binomial chain processes assuming parameter values from available literature that define the natural history of disease. Lastly, vaccinated individuals transition in a separate removed compartment if immunity is acquired. In Table 1 we report the parameter estimates used in the model.

Interventions Timeline

To realistically depict the evolution of the epidemic, a comprehensive set of policy interventions is applied to modify disease transmissibility and population mobility. On January 15, partial international travel reductions (from 10% to 40%) are applied for individuals traveling to/from China. Between January 23 and 28, flight and commuting reductions are applied to Wuhan and other subpopulations in the Hubei province to enforce government-mandated quarantines.

GLEAM

USA

Europe + Northern Africa

Southeast Asia

- • **airport**
  (transportation hub)
- □ **census cell**
  .25° x .25°
- ⬡ **geographical urban area**
  (from tessellation)

census cell population

multiscale framework

airport network

commuting network
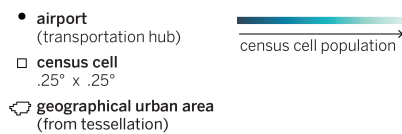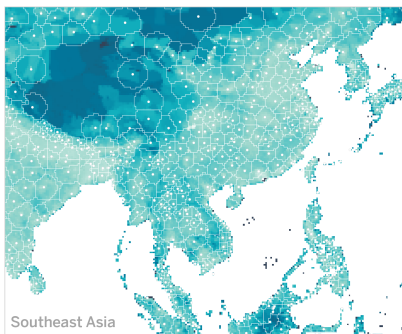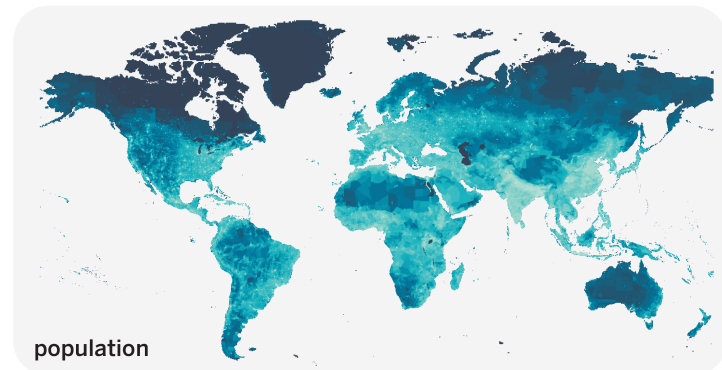
population

Figure 2: **Schematic representation of GLEAM.** (Left) Subpopulations are geographic regions formed from the Voronoi tessellation that are centered around major urban areas and transportation hubs. They are comprised of census cells that are approximately 25km x 25km. (Right) Diagram of the origin-destination airport network (long-range mobility network), the diagram of the commuting network (short-range mobility network), and the population layer of GLEAM showing the population size of census cells.
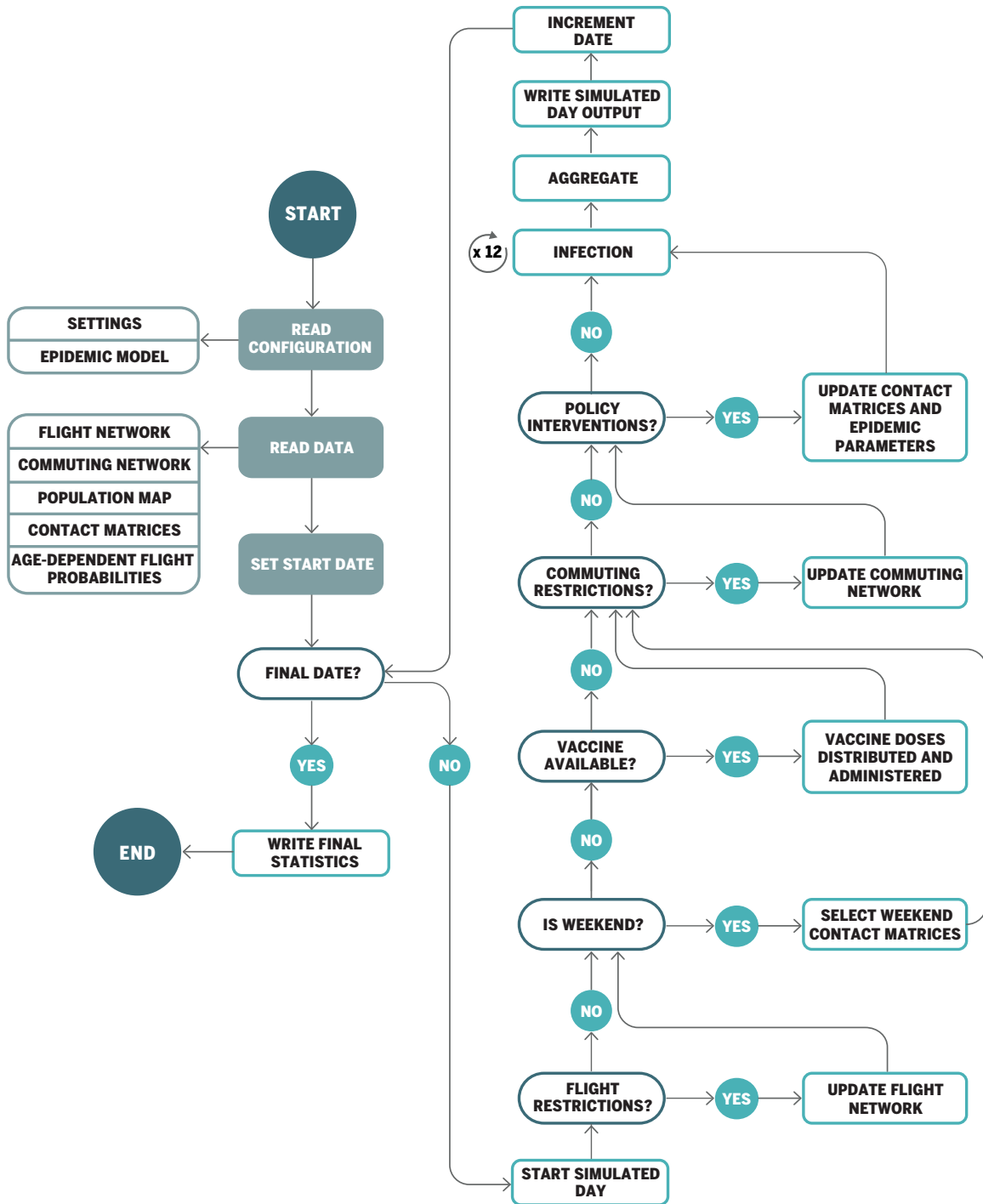
Figure 3: **Flow diagram of GLEAM's algorithm.**

Parameters	Range	Ref.
Latent period (mean)	[4 – 7] days	(*31*)
Infectious period (mean)	[2 – 4] days	(*11*)
Days until recovery	[10 – 14] days	(*11, 32*)
Generation time	[6 – 8] days	
Reproductive number	[1.6 – 3.3] in steps of 0.01	
Starting date	[2019-11-15, 2019-12-01]	(*15, 21–24*)

Table 1: **Summary of parameter ranges.** Summary of parameter ranges explored in the sensitivity analysis of the model. Reproductive number and starting date use uniform priors for the model's calibration. Reference parameters are reported in the main text.

In addition, on January 25, commuting reductions are applied also to all other subpopulations in mainland China. To do so, we collected daily travel data starting January 1, 2020 until February 25, 2020 from the Baidu Qianxi platform (*33*), which provides three mobility indices (inflow index, outflow index, and intra-city index). The indices are proxies for the number of travelers moving in, out of, and inside a city, respectively. We extracted the mobility outflow index of 27 provinces and 4 municipalities for the current year 2020 and the previous year (corresponding to the same lunar date), and then mapped all provinces and municipalities to the metapopulation structure of the model to estimate the travel flow changes during the epidemic where the travel reduction can be estimated as $1 - \frac{I_{cur}}{I_{pre}}$, where I_{cur} and I_{pre} are the mobility outflow index of current year 2020 and previous year on the same lunar date, respectively.

On February 1, due to the increasing amount of restrictions implemented by various countries and airlines (*34–39*), stronger travel reductions are applied between mainland China and the rest of the world. We use actual worldwide (international and domestic) origin-destination traffic data from the OAG database to quantify travel reductions. We also apply case detection based on travel history and additional travel bans across pairs of countries according to the Oxford COVID-19 Government Response Tracker (OxCGRT) (*40*). We account as well for the intra-country mobility and contacts reduction in workplaces and social settings (*18*) using the COVID-19 Community Mobility reports obtained from Google (*41*).

Starting in mid-March all around the world, countries started to close schools as a means to slow the spread of COVID-19. We use the timeline of school closures provided by OxCGRT (*40*). As our model considers contact matrices for different settings, namely households, schools, workplaces and the general community (*16*), we are able to quantify the resulting reduction in individuals' contacts in each one of these contexts. To implement the school closure in the United States we follow (*42*) where authors study the effects of school closure in the context of seasonal influenza epidemics. According to the date when schools closed in the different states we consider a reduction of contacts in all individuals attending an educational institution (*40, 43*). In the United States, this intervention was applied at the state level. Following the school closure, most states issued a stay-at-home order. In this case, we consider only contacts within the household and that only essential workplaces remained open. Using the COVID-19 Community Mobility reports (*41*) we were able to compute the relative reduction in the number of contacts in the workplace and the general community settings, as well as the relative reduction in the intra-country mobility. These data are available at the state level for United States, Italy and Spain among other countries, starting on February 15, 2020. The reports are updated regularly and the last

date currently used is July 31, 2020. For countries with no available mobility reports, we assume that on the date when schools are closed a 50% reduction in mobility is achieved, while an 80% reduction is considered in the case of a stay-at-home order. When the interventions are lifted, the mobility reductions are relaxed accordingly.

Global Model Calibration

The model described is stochastic and produces an ensemble of possible epidemic outcomes for each set of initial conditions. We seed the epidemic in Wuhan (China) assuming a starting date between November 15, 2019 and December 1, 2019 with 20 initial infections (*24*). Given the doubling time of the epidemic this might correspond to an outbreak that has started from mid October to late November, 2019. We simulate the epidemic scenarios by sampling the reproductive number (R_0) from a uniform prior in the range 1.6 to 3.3. We use an Approximate Bayesian Computation (ABC) Rejection Algorithm. The ABC rejection algorithm samples a set of parameter points θ (for instance R_0) according to a prior distribution and simulates the dataset E' using the model. A distance measure $s(E', E)$ determines the difference between E' and the evidence E based on a given metric. If the generated E' is outside a tolerance from the evidence E (i.e. $s(E', E) > \epsilon$) the sampled parameter value is discarded. The sampled parameters that are accepted provide an estimate of the likelihood with respect to the evidence E and allow us to calculate the posterior distribution $P(\theta, E)$. As evidence E we consider the cumulative number of SARS-CoV-2 cases internationally imported from China during the time window January 12 to January 21, 2020. The distance measure is at each date the difference between the SARS-CoV-2 cumulative imported cases generated by the model and the evidence with a tolerance provided by the under-detection interval estimated in Ref. (*27*). We also account for a non-detectable 40% rate of asymptomatic individuals (sensitivity analysis ranging from 35% to 50%) (*44, 45*). The rejection algorithm accepts only configurations that satisfy the distance measure each day. This approach allows us to calibrate the model by incorporating both the growth rate of importations and their magnitude, scaled according to the under-detection estimates. The detailed list of importation events used is provided in Table S1 of the supplementary materials of Ref. (*7*). Using the ABC calibration and the age-stratified contact matrices for China, we obtained a mean value for the basic reproductive number R_0 equal to 2.6 (*7*). This value has been used as reference in the simulations performed in this study.

List of countries with priority access to the vaccine

Albania	Greece	Portugal
Australia	Hungary	Romania
Austria	Iceland	Russian Federation
Belarus	Ireland	Serbia
Belgium	Italy	Singapore
Bosnia and Herzegovina	Latvia	Slovak Republic
Bulgaria	Lithuania	Slovenia
Canada	Luxembourg	Spain
China	Malta	Sweden
Croatia	Moldova	Switzerland
Czech Republic	Monaco	Taiwan
Denmark	Montenegro	Turkey
Estonia	Netherlands	Ukraine
Finland	North Macedonia	United Kingdom
France	Norway	United States of America
Germany	Poland	

Table 2: Countries accessing the first 2 billion vaccine doses in the uncooperative vaccination scenario.

References

1. E. Dong, H. Du, L. Gardner. An interactive web-based dashboard to track COVID-19 in real time. *The Lancet Infectious Diseases* 533–534 (2020). https://doi.org/10.1016/S1473-3099(20)30120-1.

2. D. Balcan, V. Colizza, B. Gonçalves, H. Hu, J.J. Ramasco, A. Vespignani, Multiscale mobility networks and the spatial spreading of infectious diseases. *Proceedings of the National Academy of Sciences*. **106**, 21484-21489 (2009).

3. D. Balcan, B. Gonçalves, H. Hu, J.J. Ramasco, V. Colizza, A. Vespignani, Modeling the spatial spread of infectious diseases: The GLobal Epidemic and Mobility computational model. *Journal of Computational Science* **1**, 132-145 (2010).

4. D. Balcan, H. Hu, B. Goncalves, P. Bajardi, C. Poletto, J.J. Ramasco, D. Paolotti, N. Perra, M. Tizzoni, W. Van den Broeck, V. Colizza, A. Vespignani, Seasonal transmission potential and activity peaks of the new influenza A(H1N1): a Monte Carlo likelihood analysis based on human mobility. *BMC medicine* **7**, 45 (2009).

5. Q. Zhang, K. Sun, M. Chinazzi, A. Pastore y Piontti, N.E. Dean, D.P. Rojas, S. Merler, D. Mistry, P. Poletti, L. Rossi, M. Bray, M.E. Halloran, I.M. Longini, A. Vespignani, Spread of Zika virus in the Americas. *Proceedings of the National Academy of Sciences* **114**, E4334 (2017).

6. A. P. y Piontti, N. Perra, L. Rossi, N. Samay, A. Vespignani, *Charting the Next Pandemic: Modeling Infectious Disease Spreading in the Data Science Age* (Springer, 2018).

7. M. Chinazzi, J.T. Davis, M. Ajelli, C. Gioannini, M. Litvinova, S. Merler, A.P. y Piontti, L. Rossi, K. Sun, C. Viboud, X. Xiong, H. Yu, E.M. Halloran, I.M. Longini, A. Vespignani, The effect of travel restrictions on the spread of the 2019 novel coronavirus (COVID-19) outbreak. *Science* **368**, 395–400 (2020).

8. International Air Transportation Association. https://www.iata.org/.

9. Official Aviation Guide. https://www.oag.com/.

10. M. Gatto, E. Bertuzzo, L. Mari, S. Miccoli, L. Carraro, R. Casagrandi, A. Rinaldo, Spread and dynamics of the COVID-19 epidemic in Italy: Effects of emergency containment measures. *Proceedings of the National Academy of Sciences* **117**, 10484 (2020).

11. S. M. Kissler, C. Tedijanto, E. Goldstein, Y.H. Grad, M. Lipsitch, Projecting the transmission dynamics of SARS-CoV-2 through the postpandemic period *Science* **368**, 860 (2020).

12. R. Li, S. Pei, B. Chen, Y. Song, T. Zhang, W. Yang, J. Shaman, Jeffrey, Substantial undocumented infection facilitates the rapid dissemination of novel coronavirus (SARS-CoV-2). *Science* **368**, 489 (2020).

13. J. T. Wu, K. Leung, G. M. Leung, Nowcasting and forecasting the potential domestic and international spread of the 2019-nCoV outbreak originating in Wuhan, China: a modelling study. *The Lancet*. **395** 689-697 (2020).

14. S. Lai, N. W. Ruktanonchai, L. Zhou, O. Prosper, W. Luo, J. R. Floyd, A. Wesolowski, M. Santillana, C. Zhang, X. Du, H. Yu, and A. J. Tatem, Effect of non-pharmaceutical interventions to contain COVID-19 in China. *Nature* (2020). doi.org/10.1038/s41586-020-2293-x

15. N. Imai, A. Cori, I. Dorigatti, M. Baguelin, C. A. Donnelly, S. Riley, N. M. Ferguson, "Report 3: Transmissibility of 2019-nCoV" (Imperial College London, 2020) www.imperial.ac.uk/mrc-global-infectious-disease-analysis/covid-19/report-3-transmissibility-of-covid-19/.

16. D. Mistry, M. Litvinova, M. Chinazzi, L. Fumanelli, M. F. Gomes, S. A. Haque, Q.-H. Liu, K. Mu, X. Xiong, M. E. Halloran, I.M. Longini Jr., S. Merler, M. Ajelli, A. Vespignani. Inferring high-resolution human mixing patterns for disease modeling. *arXiv* [Preprint]. 25 February 2020. https://arxiv.org/abs/2003.01214

17. H. Salje, C.T. Kiem, N. Lefrancq, N. Courtejoie, P. Bosetti, J. Paireau, A. Andronico, N. Hozé, J. Richet, C. Dubost, Y. Le Strat, J. Lessler, D. Levy-Bruhl, A. Fontanet, L. Opatowski, P.Y. Boelle, S. Cauchemez, Estimating the burden of SARS-CoV-2 in France. *Science*. **369**, 208-211 (2020).

18. J. Zhang, M. Litvinova, Y. Liang, Y. Wang, W. Wang, S. Zhao, Q. Wu, S. Merler, C. Viboud, A. Vespignani, M. Ajelli, and H. Yu. Changes in contact patterns shape the dynamics of the COVID-19 outbreak in China. *Science* (2020). doi:10.1126/science.abb8001.

19. N. G. Davies, P. Klepac, Y. Liu, K. Prem, M. Jit, CMMID COV ID-19 working group, R. M. Eggo, Age-dependent effects in the transmission and control of COVID-19 epidemics. *Nature Medicine* (2020). https://doi.org/10.1038/s41591-020-0962-9

20. Q. Bi, Y. Wu, S. Mei, C. Ye, X. Zou, Z. Zhang, X. Liu, L. Wei, S. A. Truelove, T. Zhang, W. Gao, C. Cheng, X. Tang, X. Wu, Y. Wu, B. Sun, S. Huang, Y. Sun, J. Zhang, T. Ma, J. Lessler, T. Feng, Epidemiology and transmission of COVID-19 in 391 cases and 1286 of their close contacts in Shenzhen, China: a retrospective cohort study. *The Lancet Infectious Diseases* (2020). https://doi.org/10.1016/S1473-3099(20)30287-5.

21. A. Rambaut, "Preliminary phylogenetic analysis of 11 nCoV2019 genomes, 2020-01-19" (2020); http://virological.org/t/preliminary-phylogenetic-analysis-of-11-ncov2019-genomes-2020-01-19/329.

22. K. Anderson, "Estimates of the clock and TMRCA for 2019-nCoV based on 27 genomes" (2020); http://virological.org/t/clock-and-tmrca-based-on-27-genomes/347

23. T. Bedford, R. Neher, J. Hadfield, E.Hodcroft, M. Ilcisin, N. Müller, "Genomic analysis of nCoV spread. Situation report 2020-01-23" (2020); https://nextstrain.org/narratives/ncov/sit-rep/2020-01-23

24. L. van Dorp, M. Acmana, D. Richard, L.P. Shawd, C.E. Ford, L. Ormond, C.J. Owen, J. Pang, C.C.S. Tan, F.A.T. Boshier, A.T. Ortiz, F. Balloux, Emergence of genomic diversity and recurrent mutations in SARS-CoV-2 *Infection, Genetics and Evolution : Journal of Molecular Epidemiology and Evolutionary Genetics in Infectious Diseases* **83** 104351 (2020).

25. M. Sunnåker, A.G. Busetto, E. Numminen, J. Corander, M. Foll, C. Dessimoz, Approximate Bayesian Computation, *PLoS Comput Biol*. **9**, e1002803 (2013).

26. P.M. Salazar, R. Niehus, A.R. Taylor, C.O. Buckee, M. Lipsitch. Using predicted imports of 2019-nCoV cases to determine locations that may not be identifying all imported cases. *medRxiv* 2020.02.04.20020495 [Preprint]. 11 February 2020. doi:10.1101/2020.02.04.20020495

27. R. Niehus, P. M. De Salazar, A. Taylor, M. Lipsitch, Using observational data to quantify bias of traveller-derived COVID-19 prevalence estimates in Wuhan, China. *The Lancet Infectious Diseases* (2020). https://doi.org/10.1016/S1473-3099(20)30229-2.

28. Global security index https://www.ghsindex.org/.

29. Socioeconomic Data and Applications Center (SEDAC), Columbia University. http://sedac.ciesin.columbia.edu/gpw.

30. F. Simini, M. C. González, A. Maritan, A.-L. Barabási, A universal model for mobility and migration patterns, *Nature* **484**, 96-100 (2012).

31. J. A. Backer, D. Klinkenberg, J. Wallinga, Incubation period of 2019 novel coronavirus (2019-nCoV) infections among travellers from Wuhan, China, 20–28 January 2020.*Eurosurveillance* **25**(5), 2000062 (2020). https://doi.org/10.2807/1560-7917.ES.2020.25.5.2000062

32. R. Verity, L. C. Okell, I. Dorigatti, P. Winskill, C. Whittaker, N. Imai, G. Cuomo-Dannenburg, H. Thompson, P. G. T. Walker, H. Fu, A. Dighe, J. T. Griffin, M. Baguelin, S. Bhatia, A. Boonyasiri, A. Cori, Z. Cucunubá, R. FitzJohn, K. Gaythorpe, W. Green, A. Hamlet, W. Hinsley, D. Laydon, G. Nedjati-Gilani, S. Riley, S. van Elsland, E. Volz, H. Wang, Y. Wang, X. Xi, C. A. Donnelly, A. C. Ghani, N. M. Ferguson. Estimates of the severity of coronavirus disease 2019: a model-based analysis. *The Lancet Infectious Diseases* (2020). https://doi.org/10.1016/S1473-3099(20)30243-7

33. Baidu Qianxi, http://qianxi.baidu.com/ (2020).

34. New York Times, "North Korea Bans Foreign Tourists Over Coronavirus, Tour Operator Says", https://www.nytimes.com/2020/01/21/world/asia/coronavirus-china-north-korea-tourism-ban.html (2020).

35. CNA, "Scoot cancels flights to China's Wuhan over virus outbreak", https://www.channelnewsasia.com/news/singapore/wuhan-virus-scoot-cancels-flights-mtr-train-12309076 (2020).

36. Toui tre News, "Vietnam aviation authority ceases all flights to and from coronavirus-stricken Wuhan", https://tuoitrenews.vn/news/business/20200124/vietnam-aviation-authority-ceases-all-flights-to-and-from-coronavirusstricken-wuhan/52707.html (2020).

37. Reuters, "Russia ramps up controls, shuts China border crossings over virus fears", https://www.reuters.com/article/us-china-health-russia-border/russian-regions-in-far-east-close-border-with-china-amid-coronavirus-fears-tass-idUSKBN1ZR0TU (2020).

38. Center for Disease Control, "Novel Coronavirus in China", https://wwwnc.cdc.gov/travel/notices/warning/novel-coronavirus-china (2020).

39. The Australian, "Travelers from China to be denied entry to Australia", https://www.theaustralian.com.au/subscribe/news/1/?sourceCode=TAWEB_WRE170_a&dest=https%3A%2F%2Fwww.theaustralian.com.au%2Fnation%2Ftravellers-from-china-to-be-denied-entry-into-australia%2Fnews-story%2F7b7619d44af78dd7395a934e22b52997&memtype=anonymous&mode=premium (2020).

40. T. Hale, S. Webster, A. Petherick, T. Phillips, B. Kira *Oxford COVID-19 Government Response Tracker*, Blavatnik School of Government (2020).

41. Google LLC "Google COVID-19 Community Mobility Reports", https://www.google.com/covid19/mobility/ Accessed: August 4,2020.

42. G. De Luca,K. Van Kerckhove, P. Coletti, C. Poletto, N. Bossuyt, N. Hens, V. Colizza, The impact of regular school closure on seasonal influenza epidemics: a data-driven spatial transmission model for Belgium. *BMC infectious diseases* **18**, 1-16 (2018).

43. The New York Times, "See which states and cities have told their residents to stay at home." https://www.nytimes.com/interactive/2020/us/coronavirus-stay-at-home-order.html

44. D. Oran, E. Topol, Prevalence of asymptomatic SARS-CoV-2 infection. *Ann. Internal Med* (2020,). https://doi.org/10.7326/M20-3012.

45. CDC, "COVID-19 Pandemic Planning Scenarios." https://www.cdc.gov/coronavirus/2019-ncov/hcp/planning-scenarios.html

46. E.J. Emanuel, G. Persad, A. Kern, A. Buchanan, C. Fabre, D. Halliday, J. Heath, L. Herzog, R.J. Leland, E.T. Lemango, F. Luna, M.S. McCoy, O.F. Norheim, T. Ottersen, G.O. Schaefer, K-C. Tan, C. Wellman, W. Heath J. Wolff, H.S. Richardson. An ethical framework for global vaccine allocation. *Science*, 1309–1312 (2020).

47. K Bubar, S.M. Kissler, M. Lipsitch, S. Cobey, Y.H. Grad, D.B. Larremore. Model-informed COVID-19 vaccine prioritization strategies by age and serostatus. *medRxiv* 2020.09.08.20190629v1 [Preprint]. 10 September 2020. https://doi.org/10.1101/2020.09.08.20190629